



Combined experimental and computational study on the promising monoethanolamine + 2-(ethylamino)ethanol + sulfolane biphasic aqueous solution for CO₂ absorption



Qinlan Luo ^{a,1}, Bohak Yoon ^{b,1}, Hongxia Gao ^{a,*}, Juan Lv ^a, Gyeong S. Hwang ^b, Min Xiao ^{c,*}, Zhiwu Liang ^a

^a Joint International Center for CO₂ Capture and Storage (iCCS), Hunan Provincial Key Laboratory for Cost-Effective Utilization of Fossil Fuel Aimed at Reducing CO₂ Emissions, College of Chemistry and Chemical Engineering, Hunan University, Changsha 410082, PR China

^b McKetta Department of Chemical Engineering, University of Texas at Austin, Austin, TX 78712, USA

^c Center for Applied Energy Research, University of Kentucky, Lexington, KY 40511, USA

ARTICLE INFO

Keywords:

CO₂ absorption
Biphasic solutions
Liquid–liquid phase separation
Classical molecular dynamics
Hydrogen bonds

ABSTRACT

To reduce the regeneration energy consumption for CO₂ capture, an advanced monoethanolamine (MEA) + 2-(ethylamino)ethanol (EAE) + sulfolane biphasic aqueous solution was developed, and the phase separation mechanism was explored. The effects of the concentration ratio on the phase separation behavior, CO₂ absorption performance, CO₂ loading at the phase separation point, and CO₂ desorption performance of MEA + EAE + sulfolane solutions were investigated comprehensively in experiments. The 3 M MEA + 2 M EAE + 5 M sulfolane showed the best properties with a large CO₂ loading of 0.32 mol/mol at the phase separation point and the relative low regeneration energy consumption, which is comparable to 5 M MEA in absorption with an improved desorption performance. The molecular mechanism of phase separation was revealed by molecular dynamics simulations, illustrating that strong hydrogen bonding between amine products and water and enhanced intermolecular interaction among amine products, would promote an aggregation of amine products. This study provides a promising candidate for energy-efficient CO₂ capture with molecular insights into a liquid–liquid phase separation.

1. Introduction

The CO₂ capture and storage (CCS) for post-combustion technology is one of the most promising solutions for reducing CO₂ emissions, which is the main reason for the global climate change[1]. Chemical absorption by amine scrubbing is the most mature and reliable method for CO₂ capture on a large scale (i.e., the coal-fired power plants)[2], which has been applied in the industry since 1973[3]. However, the large energy consumption in the regeneration process is a major challenge for the further application of the amine scrubbing[4]. For instance, regenerating the benchmark solvent (monoethanolamine, MEA, 30 wt%) requires 3.5–4.2 GJ/ton CO₂, accounting for 60–80% of the total energy consumption[5]. Various studies[6–8] were conducted on the development of alternative and advanced amine solutions with a fast CO₂ absorption rate, high CO₂ capacity, and low regeneration heat.

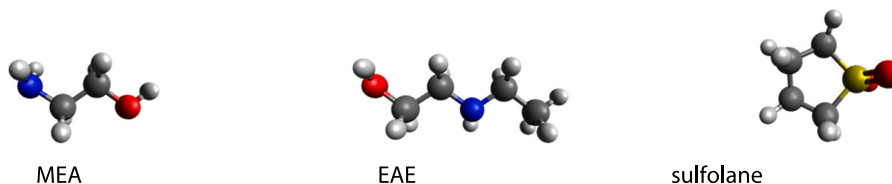
Among these new solutions, biphasic solutions have attracted much attention owing to their noticeable contribution to the reduction of regeneration energy consumption[9]. The biphasic solutions usually show a homogeneous phase prior to the absorption, and split into two CO₂-rich and CO₂-lean liquid phases after CO₂ absorption[10]. A difference in solubility between two phases causes the CO₂-rich phase to be aqueous and the CO₂-lean phase to be organic. Thereafter, only the CO₂-rich phase needs to be heated up for the regeneration, which may significantly enhance the CO₂ desorption rate, reduce the sensible heat and vaporization heat[11]. For instance, Liu et al.[12] revealed that AMP/MEA-based physical – chemical solution, showed a 36% lower regeneration energy than 30 wt% MEA.

Recent studies suggested that various amine biphasic solutions can be categorized into two types based on different kinds of phase separation promoters: primary/secondary amine + tertiary amine solutions,

* Corresponding authors.

E-mail addresses: hxgao@hnu.edu.cn (H. Gao), min.xiao2@uky.edu (M. Xiao).

¹ These authors contributed equally to this work.



Scheme 1. Molecular structure of MEA, EAE, and sulfolane, where the blue, red, grey and white balls represent N, O, C and H atoms, respectively.

primary/secondary amine + organic solvent solutions[10]. In the primary/secondary amine + tertiary amine solutions, primary/secondary amine is the absorption accelerator, while the tertiary amine is the CO₂ sinker and the regeneration promoter[13]. Zhang et al. studied the phase separation behavior of the aqueous blends comprising the primary amine (triethylenetetramine, TETA) and tertiary amines with different hydrophobicity, they investigated the absorption mechanism and proposed that the TETA + N,N-dimethylcyclohexylamine (DMCA) (4 M, 1:3) was comparable to the 5 M benchmark MEA solution for CO₂ absorption with 40% lower regeneration heat[14]. Liu et al.[15] also screened aqueous blends of 2-(diethyl-amino)-ethanol (DEEA, tertiary amine) with 12 alkanolamines, and proposed a promising DEEA + 2-((2-aminoethyl) amino) ethanol (AEEA) solvent. While using tertiary amines as the phase separation promoters has the disadvantage of high amine loss due to their high volatility and degradation rate[14]. To reduce the amine loss, researchers proposed the primary/secondary amine + organic solvent biphasic solutions using organic solvents as the phase separation promoters[16], especially the MEA-based biphasic solutions, like the MEA + 1-propanol aqueous solutions[17], MEA + sulfolane aqueous solutions[18], and MEA + diethylene glycol dimethyl ether (DGM) aqueous solutions[19].

According to our previous work[20,21] and previous studies of other groups[18,22], sulfolane was validated to be a promising phase-splitter with low vapor pressure of 0.8 Pa at 303 K. Wang et al.'s[18] results indicated that the 30% MEA + 60% sulfolane aqueous solution exhibited 35% higher CO₂ capacity and 31% lower regeneration energy than 30% MEA. Moreover, Liu et al.'s[12] work also showed that the AMP + MEA + sulfolane biphasic solution has the slightly higher CO₂ absorption rate, higher CO₂ loading and much lower regeneration heat than that of AMP + MEA solution. Therefore, the sulfolane revealed a good phase separation behavior when added into several amine aqueous solutions still with good absorption and desorption performance.

However, biphasic solutions exhibited a limited absorption rate[12] and small adjustable phase separate property[23], trade-off between the CO₂ absorption capacity and the volume ratio of the CO₂-rich phase[24] due to the single active amine used for the CO₂ capture. Therefore, primary/secondary amine A + primary/secondary amine B + organic solvent solutions may be a promising biphasic solution as it combining the advantages of amine blends and biphasic solutions, and tunable absorption rate, phase separate property and the volume ratio of CO₂-rich phase may be achieved as two amines may play different roles in absorption and phase separation. However, less work has been done on the development and investigation of those phasic solutions[13].

Therefore, in this study, a novel primary/secondary amine A + primary/secondary amine B + organic solvent biphasic solution was developed, and sulfolane was selected as the phase-splitter. Our previous experimental result[20] demonstrated that the out that MEA + sulfolane aqueous solutions exhibited the phase separation behavior, while the 2-(ethylamino)ethanol (EAE) + sulfolane aqueous solutions remained homogenous under all CO₂ loading. Thus, we explored the performance of MEA + EAE + sulfolane aqueous solutions as the biphasic absorbent for CO₂ capture. The corresponding molecular structures of these three solvents are shown in Scheme 1.

Few studies[25,26] on the molecular mechanism for the liquid–liquid phase separation have been conducted, which can provide important guidance for further developments of novel and advanced

biphasic solutions. Zhou et al.[27] used the static quantum mechanical (QM) calculations to investigate the interactions between CO₂ absorption products in diethylenetriamine (DETA) and pentamethyldiethylenetriamine (PMDETA), DETA-carbamate/DETA-carbamate, DETA-carbamate/HCO₃⁻, and HCO₃/HCO₃⁻. Kong et al.[9] explored the activation mechanism for ethanol-activated CO₂ regeneration in biphasic absorbents using QM calculation based on density functional theory (DFT), by calculating the hydrogen bond (H-bond) binding energy, H-bond length, and natural bond orbital between ions to determine the proton transfers between different product species. However, QM calculations may not accurately describe solvation effects, which can play a significant role in absorption, desorption, and phase separation of biphasic solutions. Recently, Wang et al.[28] revealed a molecular scale understanding of the phase separation mechanism underlying the CO₂ absorption in DETA + 1-propanol solutions through molecular dynamics simulations, indicating that the strong hydrogen bonds between the uncovered DETA-carbamate and pronated DETA primary cause the phase separation. Therefore, we also use molecular dynamics simulations to investigate the intermolecular interactions between products species to explore the phase separation mechanism of our biphasic solutions.

Our present work attempts to develop a novel MEA + EAE + sulfolane aqueous liquid–liquid biphasic solution, which is expected to achieve a high absorption rate, a large CO₂ loading at phase change point, and energy-efficient regeneration. Herein, the phase separation behavior of MEA + EAE + sulfolane aqueous solutions with different concentration ratio of MEA/EAE/C_{sulfolane} (C_{MEA}/C_{EAE}/C_{sulfolane}) was first investigated. Then, the influence of the C_{MEA}/C_{EAE}/C_{sulfolane} on the absorption kinetics, the phase separation behavior, and the desorption performance were assessed to develop an optimum formula of the MEA + EAE + sulfolane aqueous solution with a fast absorption rate, the late phase separation point, and low-energy penalty for CO₂ capture. Additionally, the phase separation mechanism of the MEA + EAE + sulfolane biphasic solvents was explored using molecular dynamics (MD) simulations to elucidate molecular insights into the CO₂ absorption by the biphasic primary amine + secondary amine + organic solvent + water system.

2. Experimental and computational section

2.1. Chemicals

All the chemicals used in CO₂ absorption and desorption experiments, including the monoethanolamine (MEA, ≥ 99 wt%), sulfolane (≥99 wt%), and 2-(ethylamino)ethanol (EAE, ≥ 99 wt%), were purchased from the Aladdin Reagent (Aladdin Industrial Corporation, Shanghai, China). CO₂ (≥99.99 vol%) gas and N₂ gas (≥99.999 vol%) were provided by the Changsha Rizhen Gas Co. Ltd., China. Deionized water was used in all experimental processes, which was prepared by a reverse osmosis ultrapure water equipment ($\leq 0.1 \mu\text{S}/\text{cm}$).

2.2. Absorption and desorption experiments

The CO₂ absorption and desorption performance of MEA + EAE + sulfolane aqueous solutions were investigated in the same absorption and desorption experimental systems, used in our previous studies

[20,29]. The details of the experimental systems and the experimental processes can be found in our previous work [20,30]. Based on the comprehensive comparison of phase change behavior, absorption rate, and desorption performance, our previous study [21] demonstrated that the 5 M/4M was the optimal concentration ratio of 2-methylaminoethanol (MEA) and sulfolane in MAE + sulfolane biphasic aqueous solution. Therefore, in this study, the concentration of amines (MEA + EAE) and sulfolane were also set at the range of 4 M–5 M. Various MEA + EAE + sulfolane aqueous solutions (volume of 25 ml) with different concentrations were explored in experiments, with the sulfolane concentration of 4 mol/L or 5 mol/L, and the MEA/EAE concentration range of 1 mol/L to 4 mol/L.

In the absorption experiments, the reaction temperature was set to 313.15 K and maintained by a water bath (model DC-0510, ± 0.05 °C, FDL Ltd., China). The simulated flue gas (SFG) ($P_{CO_2} = 15$ kPa, balanced by N_2) was bubbled into the absorption reactor, with the flow rate of 1000 ml/min controlled by the mass flow meters (model D07, $\pm 1.5\%$, Seven Star, China). The CO_2 concentration of both inlet gas and outlet gas was analyzed by an on-site infrared CO_2 gas analyzer (COZIR-100, $\pm 0.01\%$, GSS Ltd., U.K.). The absorption experiments were stopped as the CO_2 concentration of the outlet gas was close to that of the inlet gas ($P_{CO_2} = 15$ kPa), which indicated the saturation of CO_2 absorption in MEA + EAE + sulfolane aqueous solutions. Each absorption experiments lasted about 25 min. The CO_2 loading in solutions was calculated based on the difference of CO_2 concentration between the outlet gas and inlet gas, which was also validated by the titration using a Chittick apparatus [31]. During the absorption process, the phase separation behavior of MEA + EAE + sulfolane aqueous solutions was also observed. Thereafter, the solution was transferred to a graduated cylinder with a measuring range of 25 ml, and the volumes of the upper and lower phases were measured and recorded after the liquid–liquid phase separation. When the upper and lower phases separated, their CO_2 loading and MEA/EAE concentration were analyzed by acid titration using the Chittick apparatus.

Before the desorption experiments, the CO_2/N_2 gas was bubbled into the MEA + EAE + sulfolane solutions with the volume of 500 ml to the absorption saturation. After the phase separation, the upper phase of the MEA + EAE + sulfolane solutions was separated for desorption, and the volume of the upper phase was also measured using a graduated cylinder measuring range of 500 ml. For the desorption, the temperature was kept at 393.15 K by an oil bath (DF-101 T) with a temperature controller, and the energy consumption was also measured using an electric energy meter (Changsha instrument and meters Co. Ltd., China) with an accuracy of 0.001 kW·h. Based on our calculation, the effect of measurement accuracy on the energy consumption can be ignored, as which was less 1% of the energy consumption when the desorption rate was higher than 80%. The pure N_2 gas was used as the stripping gas with the flow rate of 500 ml/min, and the outlet gas of the desorption reactor was cooled by a condenser pipe then was sent to the on-site infrared CO_2 gas analyzer to analyze the CO_2 concentration. The desorption rate and amount can be calculated from the CO_2 concentration variation of the outlet gas with time. The CO_2 loading of the MEA + EAE + sulfolane solutions before and after desorption was measured by acid titration for the validation of the calculated CO_2 desorption amount from the outlet gas. Thereafter, the desorption rate and the CO_2 loading change was calculated by the CO_2 desorption amount in the gas.

Before the absorption and desorption experiments in MEA + EAE + sulfolane aqueous solutions, the CO_2 absorption experiment by benchmark 5 M MEA were conducted. Our experimental results indicated that the CO_2 loading around saturated absorption in 5 M MEA was 0.537 mol/mol, which was close to the result from Sholeh [32] (0.53 mol/mol). Moreover, each absorption or desorption experiment was repeated three times for a statistical significance that may verify the reliability of the experimental systems and procedures.

2.3. Data calculation

The absorption rate and desorption rate (mol/s/L) can be calculated by the following equations, respectively:

$$r_{ab} = \frac{V_{SFG}}{V_{mol} V_{sol}} \cdot \frac{(c_{in} - c_{out})}{(1 - c_{out})} \quad (1)$$

$$r_{de} = \frac{V_{N_2}}{V_{mol} V_{sol}} \cdot \frac{c_{de}}{(1 - c_{de})} \quad (2)$$

where, V_{SFG} and V_{N_2} are the volumetric flow rate of simulated flue gas in absorption (1000 ml/min) and stripping gas in desorption (500 ml/min), respectively. c_{in} and c_{out} present the volume fraction of CO_2 in the inlet gas and outlet gas of the absorption reactor, respectively. c_{de} is the volume fraction of CO_2 in the outlet gas after desorption. V_{sol} denotes the volume of aqueous solutions (L). V_{mol} is the molar volume of gas at the reaction temperature (L/mol).

The average energy consumption (EC, GJ/ton CO_2) at different desorption time can be calculated by the following equation:

$$EC_{ave} = \frac{(E_t - E_{blanket}) \times 3.6}{n_{CO_2} \times 44\bar{A} \cdot 1000} \quad (3)$$

where, E_t is the energy consumption with desorption time (t) measured by an electric energy meter, kW·h; $E_{blanket}$ donates the heat loss for blank experiments (without amine solutions) under the desorption temperature, kW·h; n_{CO_2} is the total CO_2 desorption amount with desorption time, mol.

2.4. Simulation method

Classical molecular dynamics (CMD) simulations were conducted to explore the fundamental mechanism underlying the phase separation of the rich MEA + EAE + sulfolane aqueous solutions. Diffusion properties, aggregation phenomena between absorption products, and molecular interactions among MEA-carbamate, protonated MEA, EAE-carbamate, protonated EAE, H_2O are investigated. The simulations were performed using the Large-scale Atomic/Molecular Massively Parallel Simulator (LAMMPS) program [33]. We used a modified AMBER force field for MEA-carbamate and protonated MEA with the SPC/E water model with the same force field parameters reported in our previous study [34,35]. The EAE-carbamate and protonated EAE were modeled using the General Amber Force Field. The OPLS-AA force field was used for the sulfolane molecule; more detailed information on the force field can be found in Dokko et al.'s work [36]. All atomic charges of the molecules investigated in this work were obtained from the quantum mechanical (QM) calculations at the B3LYP/6-311++G(d,p) level of theory using the Gaussian 09 program [37]. The spherical cutoffs for the Lennard-Jones and Coulomb interactions were set to 10 Å and 12 Å, respectively. Other simulation details were described in Stowe et al.'s work [38,39]. The Production runs for the diffusion coefficient values and radial distributions were carried out for 10 ns after the systems were equilibrated. The self-diffusion coefficient of all species was calculated from the mean square displacement (MSD) using the Einstein's relation [40], by fitting the slope of the calculated MSD over the averaging period. The trajectories of systems were visualized by the VMD software [41]. The hydrogen bond kinetics, the radial distribution function (RDF, $g(r)$), and the aggregation of absorption products were analyzed using the TRAVIS software [42,43]. The details of the simulations systems of the rich MEA + EAE + sulfolane aqueous solutions were shown in Table S1 in the Supporting Information, and the structures of products species were shown in Figure S1 in the Supporting Information.

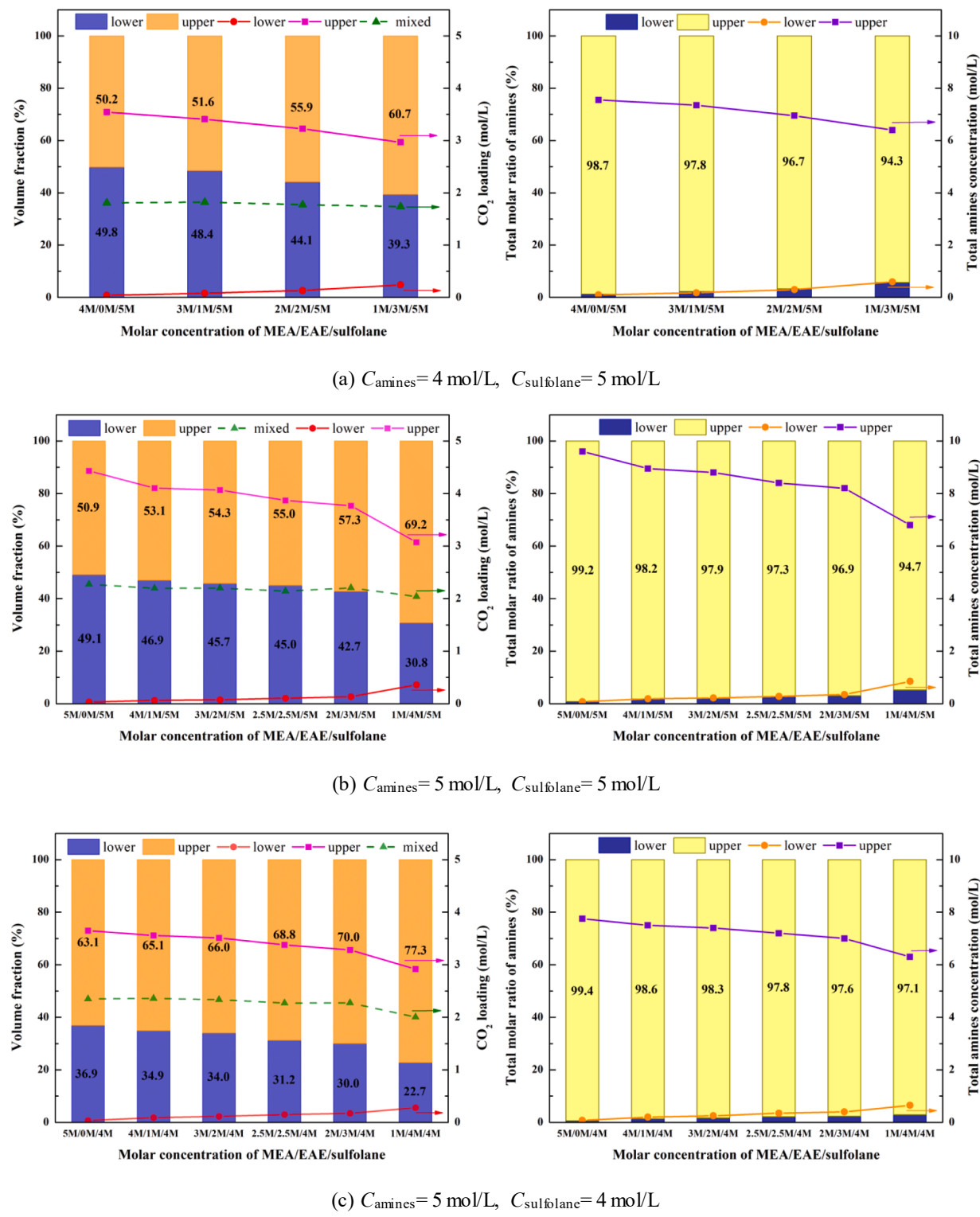


Fig. 1. Volume fraction and CO_2 loading in lower and upper phases (left), and the total molar ratio of amines and the amines concentration in lower and upper phases (right) of MEA + EAE + sulfolane aqueous solutions with different molar concentrations of MEA/EAE/sulfolane: (a) $C_{\text{amines}} = 4 \text{ mol/L}$, $C_{\text{sulfolane}} = 5 \text{ mol/L}$; (b) $C_{\text{amines}} = 5 \text{ mol/L}$, $C_{\text{sulfolane}} = 5 \text{ mol/L}$; (c) $C_{\text{amines}} = 5 \text{ mol/L}$, $C_{\text{sulfolane}} = 4 \text{ mol/L}$.

3. Results and discussion

3.1. Phase separation behavior and solution screening

The phase separation behavior of a series of MEA + EAE + sulfolane aqueous solutions was investigated after CO_2 absorption was saturated

under 313.15 K, while the molar concentration of amines (include MEA and EAE) and sulfolane varied from 4 mol/L to 5 mol/L with the MEA concentration range of 1 mol/L – 5 mol/L and the EAE concentration range of 0 mol/L – 4 mol/L. The corresponding rich MEA + EAE + sulfolane aqueous solutions contain MEA-carbamate (MEACOO^-), protonated MEA (MEA^+), EAE-carbamate (EAECOO^-), protonated EAE

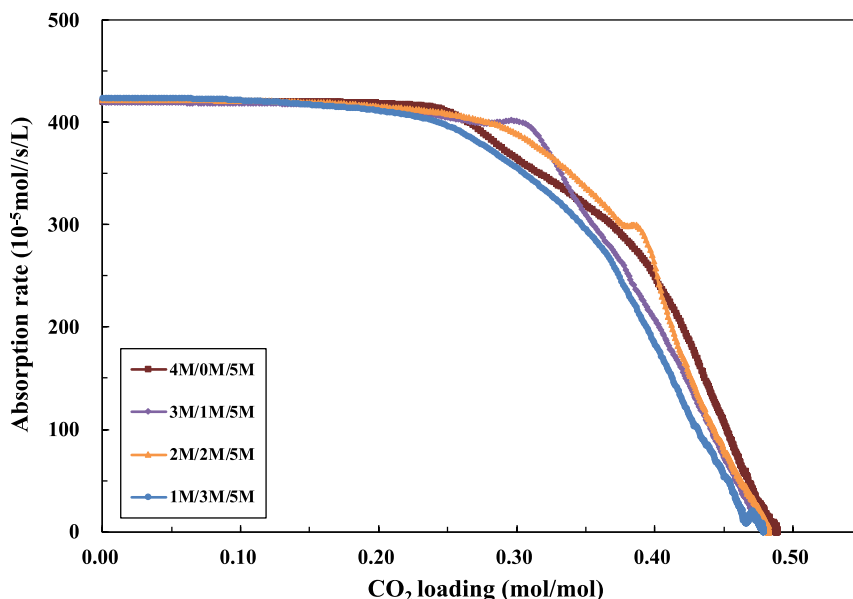
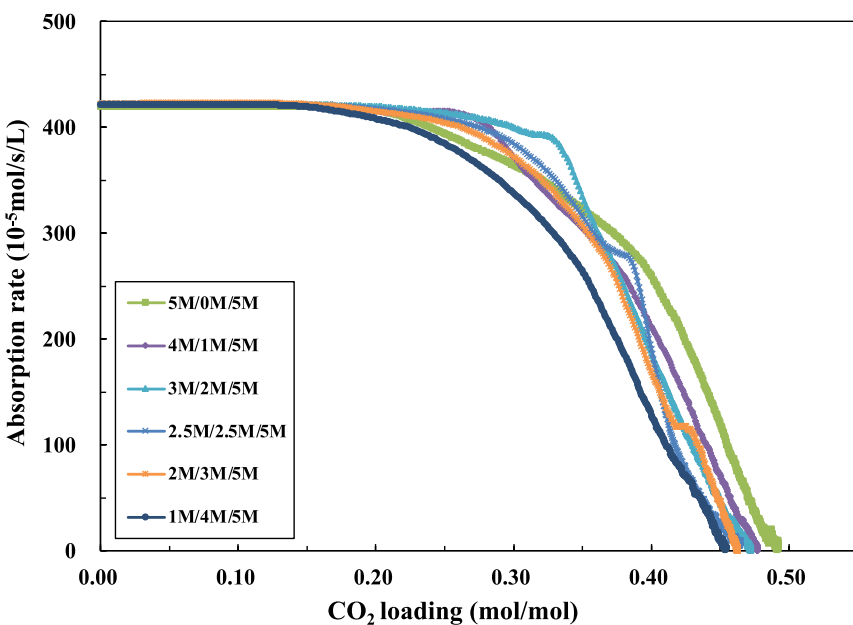
(a) $C_{\text{amines}} = 4 \text{ mol/L}$, $C_{\text{sulfolane}} = 5 \text{ mol/L}$ (b) $C_{\text{amines}} = 5 \text{ mol/L}$, $C_{\text{sulfolane}} = 5 \text{ mol/L}$

Fig. 2. With the increasing of CO_2 loading, the change tendency of absorption rate in different MEA + EAE + sulfolane aqueous solutions with different molar concentrations of MEA/EAE/sulfolane: (a) $C_{\text{amines}} = 4 \text{ mol/L}$, $C_{\text{sulfolane}} = 5 \text{ mol/L}$; (b) $C_{\text{amines}} = 5 \text{ mol/L}$, $C_{\text{sulfolane}} = 5 \text{ mol/L}$; (c) $C_{\text{amines}} = 5 \text{ mol/L}$, $C_{\text{sulfolane}} = 4 \text{ mol/L}$.

(EAEH⁺), sulfolane, water, and small amount of bicarbonate (HCO_3^-). All these MEA + EAE + sulfolane aqueous solutions will be labeled by their concentration in the following discussion, for instance, 3 M/1M/4M represents the 3 M MEA + 1 M EAE + 4 M sulfolane aqueous solution.

Our previous experimental results[20] show that the liquid–liquid phase separation can be observed in MEA + sulfolane aqueous solution after CO_2 absorption, while the EAE + sulfolane aqueous solution remain homogeneous. The different phenomenon is related to the week polarity of amino group of EAE and the poor hydrophilicity of EAE, as compared to MEA[20,21]. In this study, all MEA + EAE + sulfolane

aqueous solutions exhibit the liquid–liquid phase separation after CO_2 absorption. This result indicates that the intermolecular interactions among the product species (like hydrogen bonding and ionic bonding) in the MEA + EAE + sulfolane aqueous solutions are improved with the addition of MEA into the EAE + sulfolane aqueous solution.

Fig. 1 (a)-(c) (left) illustrate volume distribution and CO_2 loading in the lower and upper phases, and in the total solution (labeled by ‘mixed’), illustrating that a majority of CO_2 is concentrated in the upper phase after the liquid–liquid phase separation. At the same time, the molar fraction of amines and amines concentration in the lower and

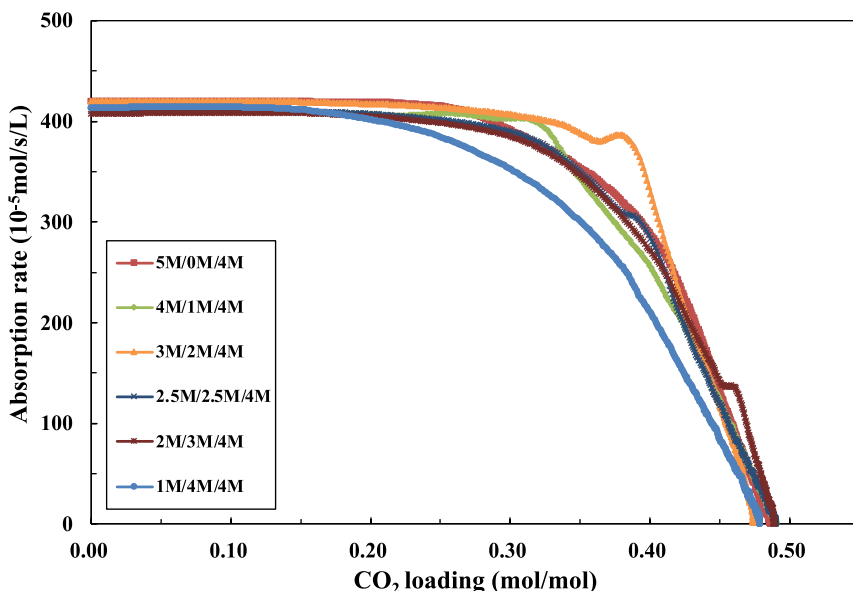
(c) $C_{\text{amines}} = 5 \text{ mol/L}$, $C_{\text{sulfolane}} = 4 \text{ mol/L}$

Fig. 2. (continued).

Table 1
Corresponding absorption time (min) and CO_2 loading (mol/mol) at the point of the phase separation of different MEA + EAE + sulfolane aqueous solutions.

Concentration of amines and sulfolane	Molar concentrations of MEA/EAE/sulfolane	Time (min)	CO_2 loading (mol/mol)
$C_{\text{amines}} = 4 \text{ mol/L}$, $C_{\text{sulfolane}} = 5 \text{ mol/L}$	4 M/0M/5M	3.33	0.2099
	3 M/1M/5M	4.42	0.2739
	2 M/2M/5M	6.30	0.3773
	1 M/3M/5M	14.33	0.4656
$C_{\text{amines}} = 5 \text{ mol/L}$, $C_{\text{sulfolane}} = 5 \text{ mol/L}$	5 M/0M/5M	4.00	0.2013
	4 M/1M/5M	4.67	0.2320
	3 M/2M/5M	6.30	0.3154
	2.5 M/2.5 M/5M	7.50	0.3611
	2 M/3M/5M	10.50	0.4204
	1 M/4M/5M	14.33	0.4401
$C_{\text{amines}} = 5 \text{ mol/L}$, $C_{\text{sulfolane}} = 4 \text{ mol/L}$	5 M/0M/4M	4.33	0.2379
	4 M/1M/4M	5.83	0.2884
	3 M/2M/4M	7.25	0.3606
	2.5 M/2.5 M/4M	8.00	0.3790
	2 M/3M/4M	11.00	0.4546
	1 M/4M/4M	15.50	0.4757

upper phases demonstrated that the upper phase has >94% of the total amines, as shown in Fig. 1 (a)-(c) (right). It should be noted that the total amines concentration is attributed to the total concentration of amine products after CO_2 absorption, while the concentration of free amines can be negligible as CO_2 absorption is saturated. Our results suggest that the upper phase is the rich MEA + EAE aqueous solution, including MEACOO^- , MEAH^+ , EAECOO^- , EAEH^+ , HCO_3^- , while the lower phase is the sulfolane aqueous solution. The primary reason that most of both CO_2 and amines are concentrated in the upper phase is attributed to the CO_2 binding with amines and the larger density of sulfolane than that of MEA/EAE aqueous solutions.

As shown in the left figures of Fig. 1 (a)-(c), at a certain concentration ratio of total amines and sulfolane ($C_{\text{amines}}/C_{\text{sulfolane}}$), with the increasing of EAE concentration and the decreasing of MEA concentration, the volume of the upper phase increases, as accompanied by the decreasing of the CO_2 loading in the upper phase. Moreover, when the concentration of total amines is 5 mol/L (in Fig. 1 (b) and (c)), the CO_2 loading in the upper phase varies from 4.43 mol/L to 3.07 mol/L or 3.65

mol/L to 2.92 mol/L, considerably higher than the CO_2 loading of 2.65 mol/L observed in the conventional 5 M MEA aqueous solution [21]. The concentrated CO_2 in the upper phase with low volume favors low energy consumption in the regeneration. A comparison between Fig. 1 (b) to Fig. 1 (c) illustrates that the volume of the lower phase at the same concentration ratio of MEA/EAE decreased when the molar concentration of sulfolane decreases from 5 mol/L to 4 mol/L.

When the EAE concentration increased at each $C_{\text{amines}}/C_{\text{sulfolane}}$, the total amine ratio of amines in the upper phase slightly decreases, while the total amines concentration of the upper phase decreases, as shown in the right figures of Fig. 1 (a)-(c). Our previous studies [20,21] point out that the addition of methyl/ethyl group would weaken the polarity of amino group and reduce the hydrophilicity of amine/amine-carbamate. Thus, the intermolecular interaction between product species in EAE- $\text{CO}_2\text{-H}_2\text{O}$ system (i.e., between EAE-carbamate and pronated EAE pair, EAE-carbamate and water pair, and pronated EAE and water pair) is stronger than that in MEA- $\text{CO}_2\text{-H}_2\text{O}$ system (i.e., between MEA-carbamate and pronated MEA pair, MEA-carbamate and water pair, pronated MEA and water pair), which can clearly explain the phenomenon aforementioned. Therefore, we can obtain more concentrated CO_2 and higher amines concentration in the upper phase with the higher MEA concentration ratio.

3.2. Effect of the concentration proportion of MEA/EAE/sulfolane on the absorption performance

To explore the absorption performance of MEA + EAE + sulfolane aqueous solutions with different C_{MEA} , C_{EAE} and $C_{\text{sulfolane}}$, the CO_2 concentration of inlet gas and outlet gas during the absorption process was recorded in real-time. From the experiment, the absorption rate and CO_2 loading can be calculated based on the CO_2 concentration difference between the inlet gas and outlet gas; the final CO_2 loading after the absorption process can also be verified by the acid titration of the rich MEA + EAE + sulfolane aqueous solutions. The absorption rate (mol/s/L) curve with the CO_2 loading (mol/mol) of different MEA + EAE + sulfolane aqueous solutions is shown in Fig. 2.

The absorption rate of different MEA + EAE + sulfolane aqueous solutions reveals the same variation tendency with the change of CO_2 loading. All the MEA + EAE + sulfolane aqueous solutions have the

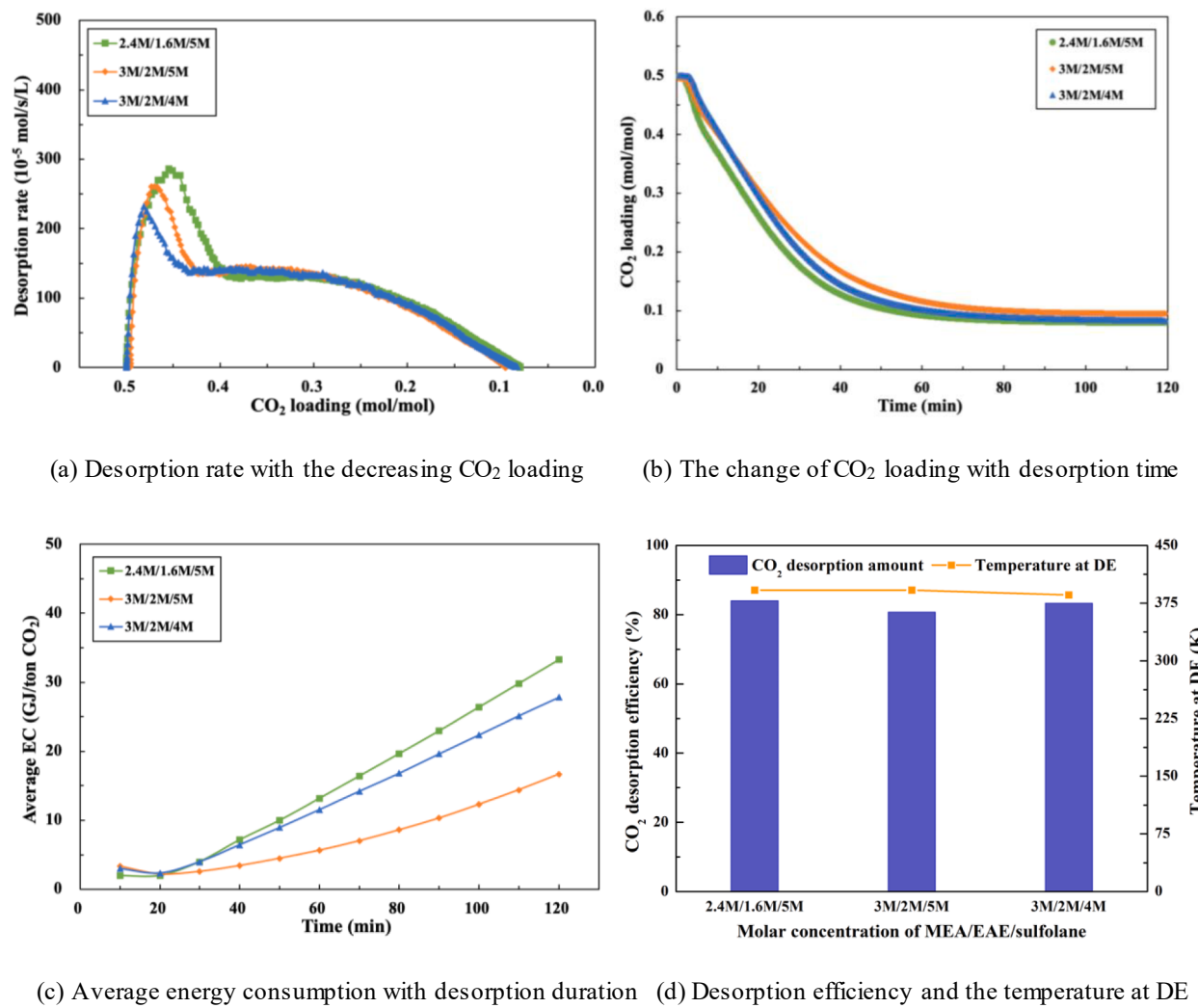


Fig. 3. Desorption performance of different MEA + EAE + sulfolane aqueous solutions with different molar concentrations of MEA/EAE/sulfolane: (a) Desorption rate with the decreasing CO₂ loading; (b) The change of CO₂ loading with desorption time; (c) Average energy consumption with desorption duration; (d) Desorption efficiency and the temperature at DE.

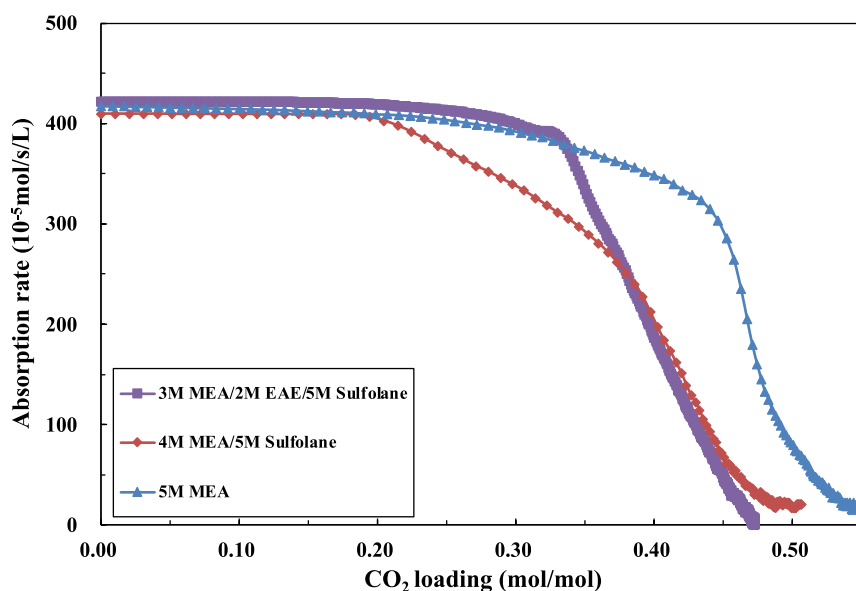


Fig. 4. Absorption performance of MEA + EAE + sulfolane aqueous solution compared to that of MEA and MEA + sulfolane solutions.

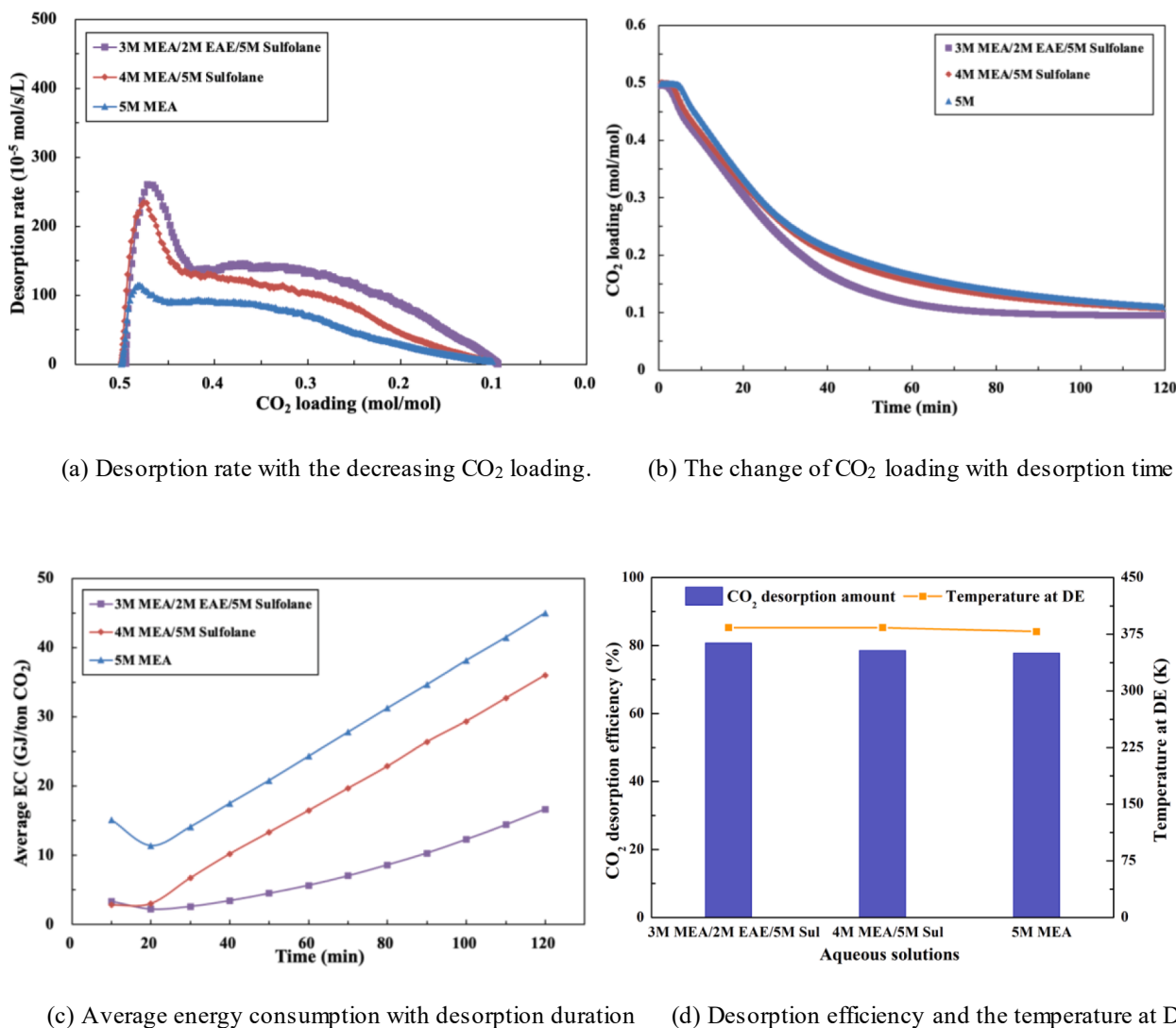


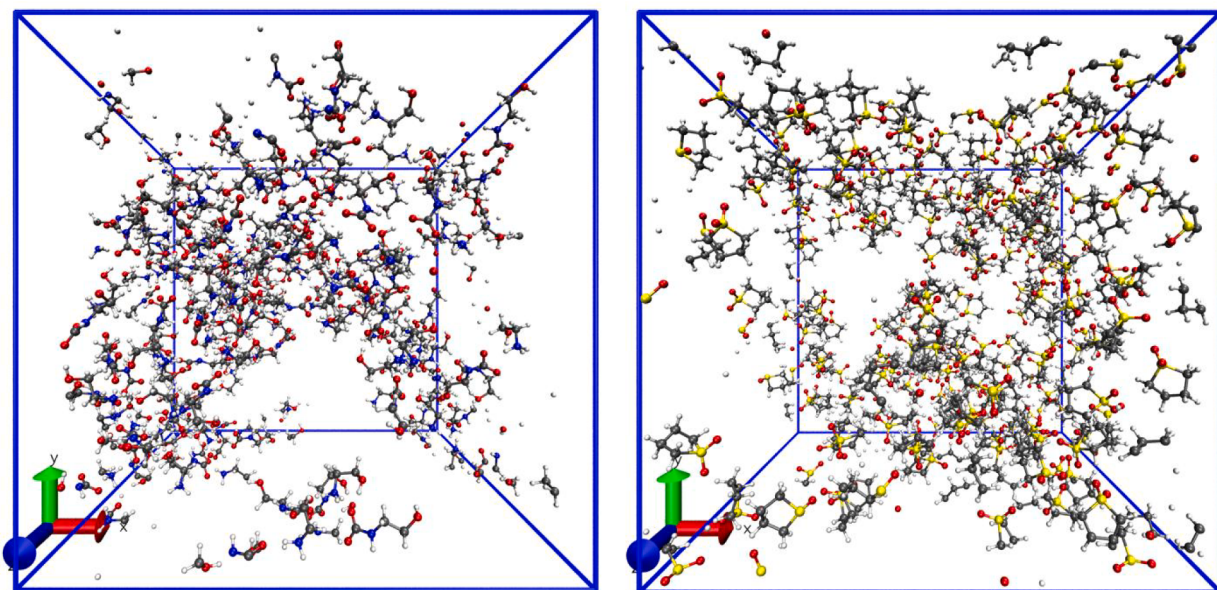
Fig. 5. Desorption performance of MEA + EAE + sulfolane aqueous solution compared to that of MEA and MEA + sulfolane solutions: (a) Desorption rate change with the decreasing CO_2 loading; (b) The change of CO_2 loading with desorption time; (c) Average energy consumption with different CO_2 desorption duration; (d) Desorption efficiency and the temperature at DE

same initial absorption rate around 0.0041–0.0042 mol/s/L, while all the absorption rates remain unchanged when the CO_2 loading is smaller than 0.15 mol/L. This can be explained by the phenomenon at the beginning of the absorption process that the absorption rate is limited by the CO_2 concentration in the SFG or the flow rate of SFG, as the concentration of amines in solutions is sufficiently high at the beginning of the absorption. Nevertheless, further assessments on the tendency of similar initial absorption rate of different solutions are beyond the scope of this study, and thus not investigated further, as the chemical reaction between CO_2 and solutions is the main focus of this study. When the CO_2 loading is around 0.2 mol/L, the absorption rate starts to decrease as the consumption of free amines in solutions. With the further increase of CO_2 loading, the absorption rate sharply declines; at this stage, the absorption rate is controlled by the chemical reactions between CO_2 and amines in the liquid phase. The CO_2 loading of different MEA + EAE + sulfolane aqueous solutions falls in the range of 0.45 – 0.49 mol/mol. The small difference is related to the concentration ratio of MEA and EAE ($C_{\text{MEA}}/C_{\text{EAE}}$), which can be explained by higher CO_2 absorption-reaction activity of MEA in than that of EAE.

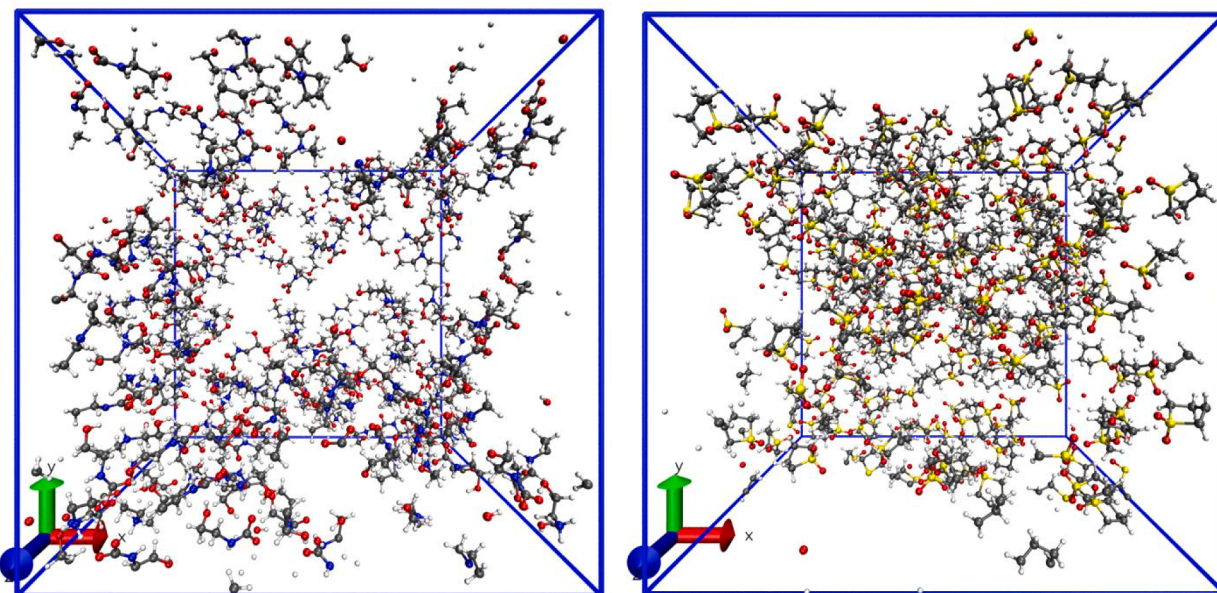
It is worth to be noted that each absorption rate curve of each MEA + EAE + sulfolane aqueous solution has an inflection point, at which the liquid–liquid phase separation is observed around. After the inflection

point, the absorption rate decreases rapidly, showing that the MEA + EAE + sulfolane solutions are less suitable for the CO_2 absorption after the phase separation. For MEA + sulfolane solutions, the fluctuation of absorption rate around the inflection point is not as noticeable, as shown in Figure S1 (supporting information), but the phase separation phenomenon can still be observed. The phenomenon may relate to the long phase change time of MEA + sulfolane solutions, which means it would take the MEA + sulfolane solutions longer time to reach total liquid–liquid phase separation, and during the process the effect of phase separation on absorption rate was less significant. As shown in Fig. 2, the phase separation of different MEA + EAE + sulfolane solutions may occur under different CO_2 loading. The position of inflection points in different MEA + EAE + sulfolane solutions is also shown in Figure S1, and the corresponding time and CO_2 loading at the inflection point of phase separation is presented in Table 1.

The CO_2 loading at the phase separation point of MEA + sulfolane solutions is relatively low, at the range of 0.201–0.238 mol/mol. It can be noticed that the corresponding time and CO_2 loading of the phase separation increased, with the decreasing $C_{\text{MEA}}/C_{\text{EAE}}$ (i.e., from 4 M/0M/5M to 1 M/3M/5M, from 5 M/0M/5M to 1 M/4M/5M, and from 5 M/0M/4M to 1 M/4M/4M). This indicates that the phase separation of MEA + EAE + sulfolane solutions can be hindered by the addition of



(a) Aggregation of amine products (left) and sulfolane (right) in 5M MEA + 5M sulfolane



(b) Aggregation of amine products (left) and sulfolane (right) in 3M/2M/5M

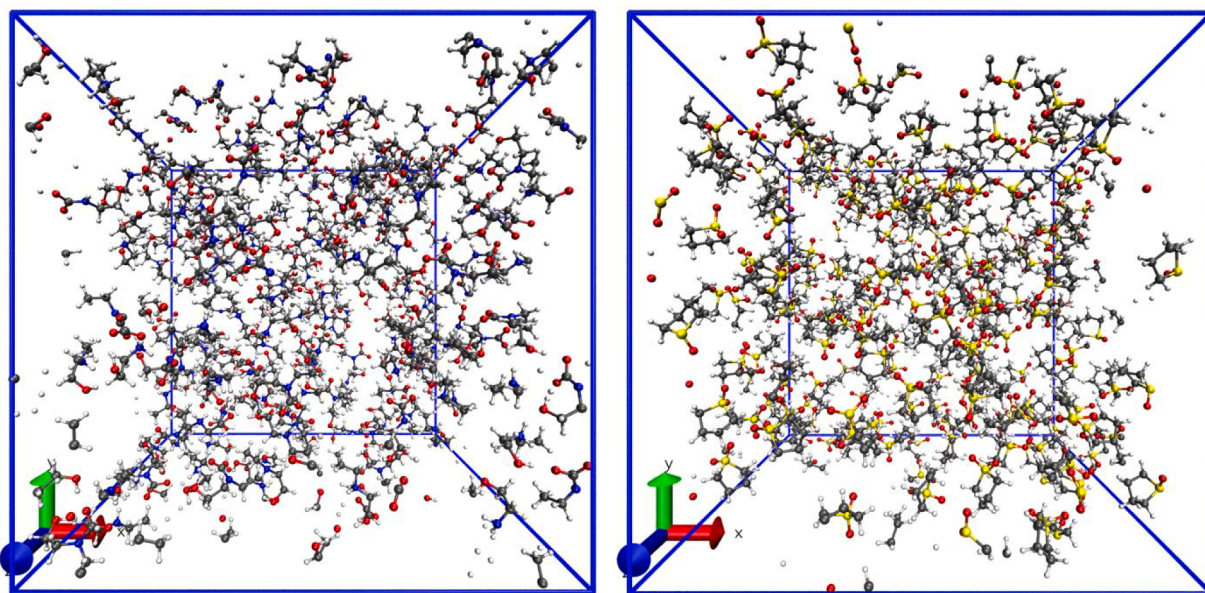
Fig. 6. Aggregation of amine products ($\text{MEACOO}^-/\text{MEA}\text{H}^+$ / $\text{EAECOO}^-/\text{EAEH}^+$) (left) and sulfolane (right) in $\text{MEA} + \text{sulfolane}$ or $\text{MEA} + \text{EAE} + \text{sulfolane}$ aqueous solutions: (a) 5 M MEA + 5 M sulfolane; (b) 3 M/2M/5M; (c) 1 M/4M/5M. The details of the structures of amine products can be found in Figure S1 in the Supporting Information.

EAE. These phenomena are consistent with the results in extreme cases that the phase separation start at low CO_2 loading in $\text{MEA} + \text{sulfolane}$ solutions, while EAE + sulfolane solutions remain homogeneous at the whole absorption process[20].

These phenomena are observed due to the stronger polarity in the absorption products (MEACOO^- and MEAH^+) of MEA than in the absorption products (EAECOO^- , EAEH^+) of EAE. The lower polarity in the EAE product pair ($\text{EAECOO}^-/\text{EAEH}^+$) can be understood that an ethyl group in $\text{EAECOO}^-/\text{EAEH}^+$ is an anionoid inductive substituent that may induce a negative charge on the adjacent N atom (i.e., inductive effect) [44], as compared to $\text{MEACOO}^-/\text{MEA}\text{H}^+$. More detailed molecular

structures of the two product pairs are shown in Scheme S1 (Supporting Information).

In addition, the phase separation becomes hindered with the longer absorption time and the higher CO_2 loading at a fixed the $C_{\text{MEA}}/C_{\text{EAE}}$, when the $C_{\text{sulfolane}}$ decreases from 5 mol/L to 4 mol/L. This is due to the tendency that the phase separation is also related to the hydrophobicity of the sulfolane; thus, the $\text{MEA} + \text{EAE} + \text{sulfolane}$ solutions with the higher sulfolane concentration would be more prone to phase separation. Our results clearly show that, the $\text{MEA} + \text{EAE} + \text{sulfolane}$ aqueous solutions can split into two liquid phases at a higher CO_2 loading under the lower MEA concentration, the higher EAE concentration, and the



(c) Aggregation of amine products (left) and sulfolane (right) in 1M/4M/5M

Fig. 6. (continued).

lower sulfolane concentration.

As shown in Fig. 2 (a), (b) and (c), the 2 M/2M/5M, 3 M/2M/5M, and 3 M/2M/4M show the best absorption performance, respectively, whereby the absorption rate is high, and the premature decreasing brought by the phase separation is not observed. Therefore, 3/2 (or close to 3/2) was the best C_{MEA}/C_{EAE} under different concentrations of amines and sulfolane.

3.3. Effect of the concentration ratio of amines and sulfolane on the desorption performance.

Based on our findings as described earlier, the desorption performance of MEA + EAE + sulfolane under the best concentration ratio ($C_{MEA}/C_{EAE} = 3/2$) is explored in experiments, including 2.4 M/1.6 M/5M, 3 M/2M/5M, and 3 M/2M/4M. The volume of the upper phase of the 2.4 M/1.6 M/5M, 3 M/2M/5M, and 3 M/2M/4M was 265 ml, 271 ml, and 330 ml, respectively.

The desorption rate of different MEA + EAE + sulfolane solutions with the change of the CO_2 loading is shown in Fig. 3 (a). With the decreasing of the CO_2 loading, the desorption rate of all the three MEA + EAE + sulfolane solutions show an identical variation tendency, of which the desorption rate reaches the maximum at the CO_2 loading of 0.475–0.450 mol/mol followed by a sharp decrease, and then slowly declines when the CO_2 loading is less than 0.40 mol/mol. The variation tendency can be understood into the two regeneration stages: (a) at CO_2 loading of 0.5–0.4 mol/mol, the bicarbonate in the rich solutions resolve first due to its lower thermodynamics stability, and (b) at CO_2 loading lower than 0.4 mol/mol, the carbamates (MEACOO^- and EAECOO^-) start to break down. The change of CO_2 loading in rich solutions with the desorption time is illustrated in Fig. 3 (b). It also can be found that CO_2 loading shows a more noticeable decrease at the beginning of the desorption process. Among the three solutions, the 2.4 M/1.6 M/5M with the lowest $C_{\text{amines}}/C_{\text{sulfolane}}$ shows the highest desorption rate.

Based on the measurement of electric energy consumption and desorption CO_2 amount, the average energy consumption (EC) presenting the average energy amount (GJ) needed for the releasing of per ton CO_2 from the rich solution is calculated. The curves of average EC with the change of desorption duration are illustrated in Fig. 3 (c). The average EC slightly decreases at the beginning, then increases, and

reaches the minimum at 20 mins. During the desorption process, water evaporation may cause a large amount of energy consumption. The CO_2 desorption amount decreased after 20 mins, while a large amount of water evaporating into the gas phase is still present, thereby leading to a continuous increase of the average EC.

In addition, the difference of the average EC among the three solutions can be attributed to the different boiling points of MEA + EAE + sulfolane solutions. The boiling point of MEA, EAE, and sulfolane are 443.15 K, 442.15 K, and 558.15 K, respectively. Therefore, the solution with the lower $C_{\text{amines}}/C_{\text{sulfolane}}$ has a higher azeotropic point, leading to a lower vapor (especially water-vapor) pressure and a higher temperature at the desorption ending (DE), as shown in Fig. 3 (d).

For the CO_2 desorption efficiency, as also displayed in Fig. 3 (d), the three solutions yield an order of 2.4 M/1.6 M/5M > 3 M/2M/4M > 3 M/2M/5M, with small difference at the range of 80.8% – 84.0%. When combined with the order of the energy consumption needed for the water evaporation: 3 M/2M/4M > 3 M/2M/5M > 2.4 M/1.6 M/5M, related to the azeotropic point of solutions, the average EC of solutions showed the order of: 2.4 M/1.6 M/5M > 3 M/2M/4M > 3 M/2M/5M. The average EC of 3 M/2M/5M in 120 mins is predicted to be 16.66 GJ/ton CO_2 , which is only 50% and 60% of the average EC of 2.4 M/1.6 M/5M and 3 M/2M/4M, respectively. Since the desorption experiments were carried out in a batch reactor, the value is only used for relative comparison in this work.

Overall, the 3 M/2M/5M shows improved absorption and desorption performance, with the concentrated CO_2 loading of 4.07 mol/L and 97.9% amine in the upper phase, high absorption rate, large CO_2 loading (0.315 mol/mol) of the phase separation point, high desorption rate, sufficient desorption efficiency (80.8%), and the relative low regeneration energy cost.

3.4. Comparison of the absorption and desorption performance with other aqueous solutions

To evaluate the advantages of the MEA + EAE + sulfolane aqueous solutions for the CO_2 capture, the absorption and desorption performance of 3 M/2M/5M is compared with that of benchmark 5 M MEA. The 4 M MEA + 5 M sulfolane shows the best absorption and desorption performance compared to other two-solvent biphasic blends (like MEA/

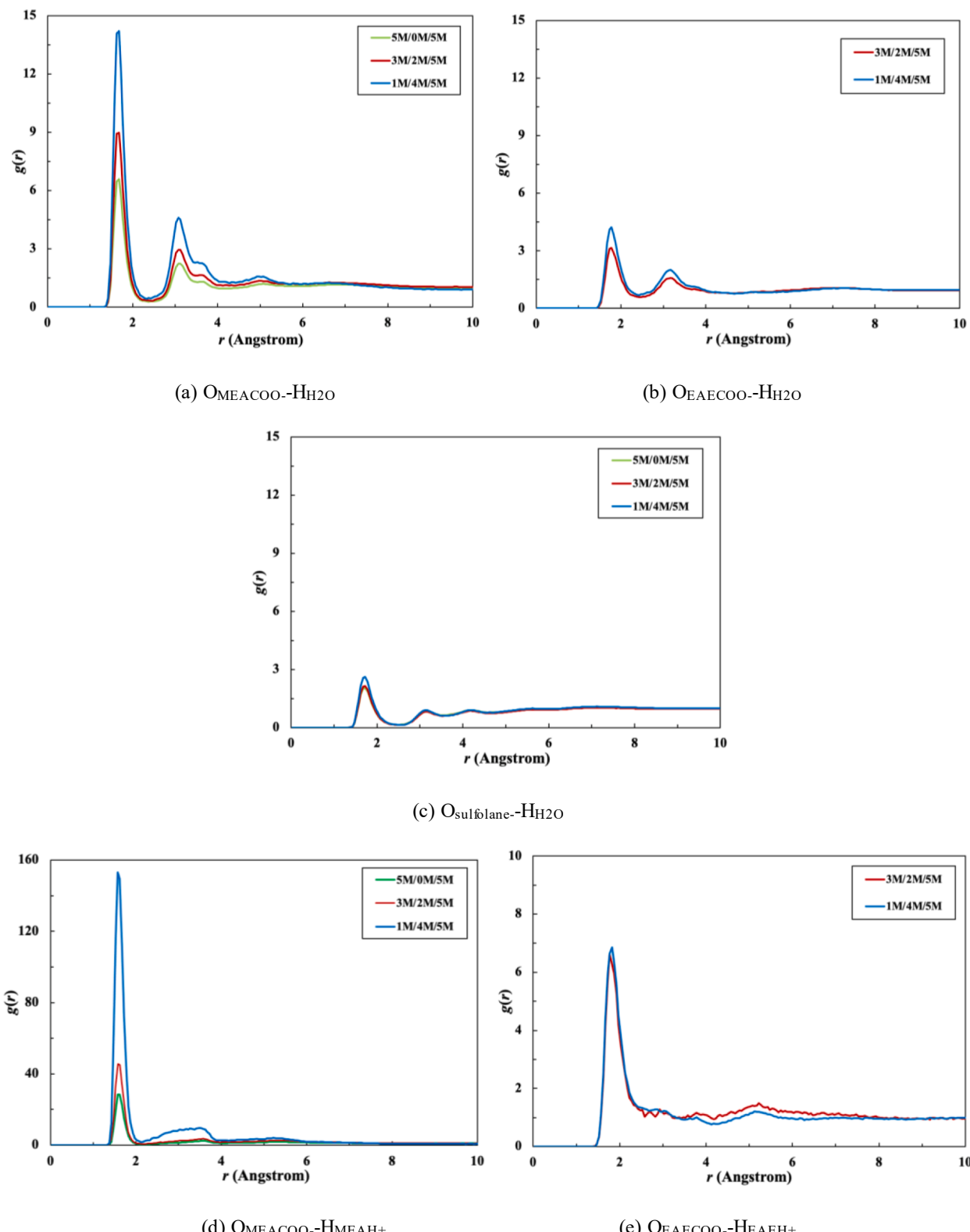


Fig. 7. RDFs of different pairs for MEA + sulfolane and MEA + EAE aqueous systems: (a) RDFs of O atom from –COO group in MEACOO[–] and H atom in H₂O; (b) RDFs of O atom from –COO group in EAECOO[–] and H atom in H₂O; (c) RDFs of O atom from -SOO group in sulfolane and H atom in H₂O; (d) RDFs of O atom from –COO group in MEACOO[–] and H atom from –OH group in MEA⁺; (e) RDFs of O atom from –COO group in EAECOO[–] and H atom from –OH group in EA⁺; (f) RDFs of O atom from –COO group in MEACOO[–] and H atom from –OH group in EAEH⁺; (g) RDFs of O atom from –COO group in EAECOO[–] and H atom from –OH group in MEA⁺.

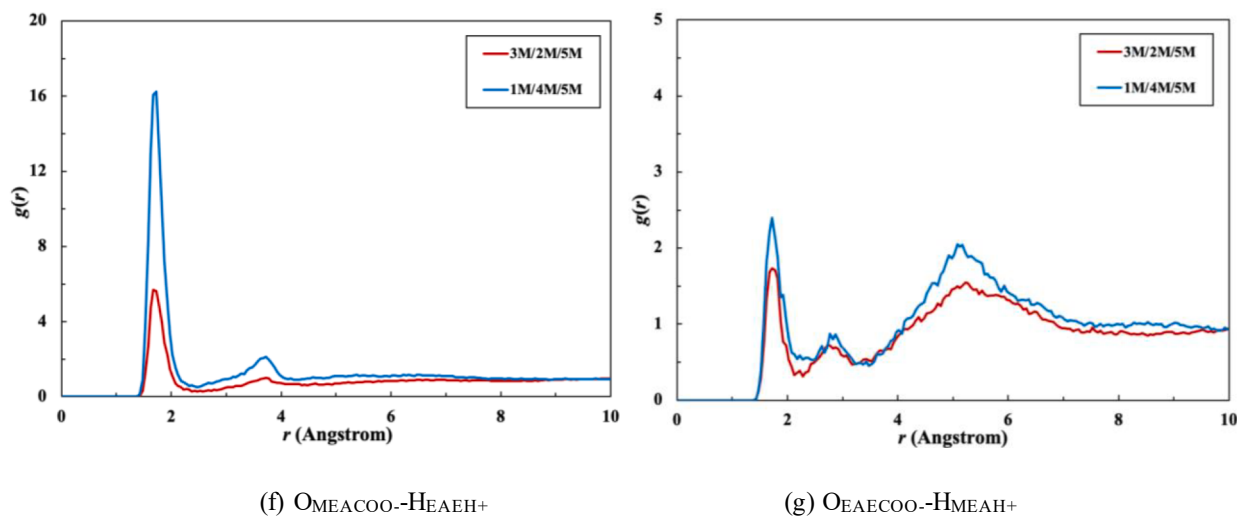


Fig. 7. (continued).

Methanol, MEA/DMAB, DETA/sulfolane), proposed by the Wang et al. [18], thus, it is also chosen as the reference in this study.

As shown in Fig. 4, the three solutions reveal an order of absorption rate: 5 M MEA > 3 M/2M/5M > 4 M MEA + 5 M sulfolane. The 3 M/2M/5M and 4 M MEA + 5 M sulfolane solutions undergo the phase separation at the CO₂ loading of 0.32 mol/mol and 0.21 mol/mol, respectively. Before the phase separation, the 3 M/2M/5M demonstrate the highest absorption rate due to its high amines concentration as compared to 4 M MEA + 5 M sulfolane and enhanced interaction between MEA and EAE as compared to 5 M MEA. For the interaction between MEA and EAE, our previous kinetics study [45] reveals that the EAE can play an important role of proton acceptor for the deprotonation of MEA-zwitterion, releasing more MEA to react with CO₂ to form MEA-zwitterion. Moreover, EAE ($pK_a = 10.0$) shows a stronger basicity than MEA ($pK_a = 9.5$), improving the reaction kinetics of MEA-zwitterion deprotonation. Therefore, the interaction between MEA and EAE induces the higher absorption rate of 3 M/2M/5M as compared to 5 M MEA.

Before the desorption experiments, the rich 3 M/2M/5M, 4 M MEA + 5 M sulfolane, and 5 M MEA solutions were prepared by the continuously bubbling of CO₂ until the saturation of absorption. Thereafter, the upper phase of the 3 M/2M/5M ($V_{upper} = 270$ ml) and 4 M MEA + 5 M sulfolane solution ($V_{upper} = 250$ ml), and the total 5 M MEA solution ($V_{soln} = 500$ ml) were heated to 393.15 K for the desorption.

As illustrated in Fig. 5 (a) and (c), the biphasic solutions (3 M/2M/5M and 4 M MEA + 5 M sulfolane) show a much higher desorption rate and the much lower average EC than the traditional 5 M MEA solution, due to the concentrated amines in the upper phase and less solution volume for desorption. The desorption rate of the three solutions is in the order of 3 M/2M/5M > 4 M MEA + 5 M sulfolane > 5 M MEA, consistent with the change of CO₂ loading in solutions, as shown in Fig. 5 (b). The total CO₂ desorption efficiency of the 3 M/2M/5M is 80.8%, a bit higher than that of 5 M MEA (77.8%) and 4 M MEA + 5 M sulfolane (78.6%).

Our results demonstrate that, the 3 M/2M/5M has a better absorption and desorption performance than the 5 M MEA solution and the 4 M MEA + 5 M sulfolane solution, which can be a promising candidate for the advancement of CO₂ capture techniques with high absorption rate and low energy consumption of regeneration.

3.5. The phase separation mechanism

To investigate the intermolecular interactions among products and phase separation mechanism in CO₂-loaded MEA + EAE + sulfolane aqueous solutions, classical molecular dynamics (CMD) simulations of

three aqueous solutions (5 M MEA + 5 M sulfolane, 3 M/2M/5M, 1 M/4M/5M) with the CO₂ loading of 0.5 mol/mol were performed using the LAMMPS. The calculated density of solutions is comparable to the experimental density, verifying the reliability of our simulations, as shown in Table S1 in the Supporting Information.

The spatial distributions of amines products (MEACOO⁻/MEA⁺/EAECOO⁻/EAEH⁺) and sulfolane of different simulation systems, after 10 ns production runs followed by the equilibration runs under canonical ensemble, are displayed in Fig. 6. The aggregation of amine products and the self-aggregation of sulfolane, as well as the immiscible phenomenon between amines products and sulfolane can be found in each system. Meanwhile, the aggregation of MEACOO⁻/MEA⁺ in the 5 M MEA + 5 M sulfolane is more noticeable than that of MEACOO⁻/MEA⁺/EAECOO⁻/EAEH⁺ in the 3 M/2M/5M and 1 M/4M/5M, in accordance with higher total amine concentration in the upper phase of 5 M/0M/5M than that of 3 M/2M/5M and 1 M/4M/5M as shown in Fig. 1 (b) (right). The self-diffusion coefficients of different species are also calculated from the mean-square displacements (MSD), as shown in Table S2. This result also indicates that the phase separation of the CO₂-loaded MEA + EAE + sulfolane aqueous solutions is strongly related to the aggregation of amines products.

To further explore the nature of intermolecular interaction in the CO₂-loaded MEA + EAE + sulfolane, the radial distribution function (RDF, $g(r)$) of different pairs between different species are analyzed, as displayed in Fig. 7. The RDF indicates the probability of the observed atom at the distance r from the reference atom, given by the following equation:

$$g(r) = \langle \frac{n(r, r + dr)}{\rho} dr \rangle \quad (1)$$

where, $n(r, r + dr)$ is the number of the observed atom in a spherical shell of thickness dr at the distance r from the reference atom; ρ presents the bulk number density of the observed atom.

Fig. 7 (a), (b), and (c) present the RDF curves between MEACOO⁻, EAECOO⁻, and sulfolane with H₂O, respectively. All RDF curves reveal sharp maxima at an r interval of 1.6–1.7 Å, indicating strong hydrogen-bonded pairs between the O atom from -COO group in MEACOO⁻/EAECOO⁻ or O atom from -SOO group in sulfolane and surrounding water molecules (H atom). As can be illustrated from Fig. 7 (a), (b), and (c), the maximum values of the peak in each simulation system are in the order of OMEACOO-H₂O > OEAECOO-H₂O > O_{sulfolane}-H₂O, indicating that the hydrogen bond between MEACOO⁻ and H₂O is stronger than that between EAECOO⁻ and H₂O or that between sulfolane and H₂O. Thus, the hydrophilicity of species is in the order of MEACOO⁻ >>

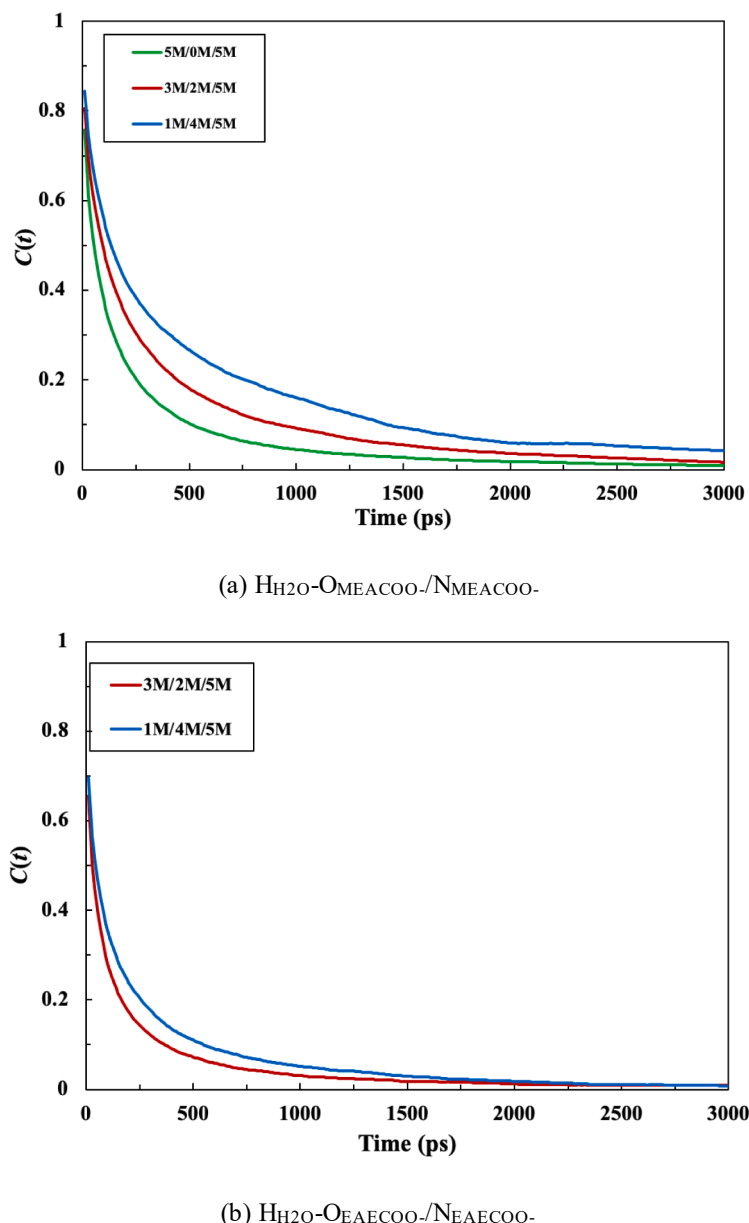


Fig. 8. Hydrogen bond autocorrelation functions for the hydrogen bonds between MEACOO^- , EAECOO^- or sulfolane and surrounding water molecules: (a) pair of H atom in H_2O and O atom from $-\text{COO}$ group in MEACOO^- or N in MEACOO^- ; (b) pair of H atom in H_2O and O atom from $-\text{COO}$ group in EAECOO^- or N in EAECOO^- ; (c) pair of H atom in H_2O and O atom from $-\text{SOO}$ group in sulfolane.

$\text{EAECOO}^- >$ sulfolane. This can explain the experimental phenomenon that the CO_2 -loaded MEA + sulfolane has the phase separation behavior while the CO_2 -loaded EAE + sulfolane stays in the homogeneous phase. The area under the first peak of $g(r)$ to $2.4\text{--}2.5 \text{ \AA}$ for $\text{O}_{\text{MEACOO}-}\text{--H}_{\text{H}_2\text{O}}$ pairs in 5 M/0M/5M, 3 M/2M/5M, and 1 M/4M/5M yields coordination numbers (CNs) of 1.22, 1.08 and 0.82, respectively; $\text{O}_{\text{EAECOO}-}\text{--H}_{\text{H}_2\text{O}}$ in 3 M/2M/5M and 1 M/4M/5M yields the CNs of 0.65 and 0.40; $\text{O}_{\text{sulfolane}-}\text{--H}_{\text{H}_2\text{O}}$ in 5 M/0M/5M, 3 M/2M/5M, and 1 M/4M/5M yields the CNs of 0.52, 0.36 and 0.21, respectively, as shown in Table S3. This change clearly suggests that both MEACOO^- and EAECOO^- forms fewer hydrogen bonds (HBs) at lower $\text{C}_{\text{MEA}}/\text{C}_{\text{EAE}}$, consistent with the lower total amines' concentration in the upper phase (as shown in Fig. 1 (b)). As a result, the fewer HBs forming between sulfolane and water induces smaller volume of the lower phase (as shown in Fig. 1 (c)).

As illustrated in Fig. 7 (d), (e), (f), and (g), the first peak around 1.6 \AA of RDF curves implies the strong hydrogen bonding interaction between

the O atom of $-\text{COO}$ group in $\text{MEACOO}^-/\text{EAECOO}^-$ and the H atom of $-\text{OH}$ group in $\text{MEA}\text{H}^+/\text{EA}\text{EH}^+$. The maximum values of the first peak in every system indicates the strength of intermolecular interaction between amines products, which is in the order of $\text{O}_{\text{MEACOO}-}\text{--H}_{\text{MEA}\text{H}^+} > \text{O}_{\text{MEACOO}-}\text{--H}_{\text{EA}\text{EH}^+} > \text{O}_{\text{EAECOO}-}\text{--H}_{\text{EA}\text{EH}^+} > \text{O}_{\text{EAECOO}-}\text{--H}_{\text{MEA}\text{H}^+}$. This can be strongly related to the stronger polarity of MEA and the steric hindrance effect of EAE hindering the approaching of other molecules.

The dynamics of the hydrogen bonds between MEACOO^- , EAECOO^- or sulfolane and surrounding water molecules are further examined by calculating the intermittent HB correlation function $C(t)$, which describes the probability of the selected atom pairs remaining hydrogen bonds at time t , and can be defined by the following equation[46]:

$$C(t) = \frac{\langle \delta h(t) \delta h(0) \rangle}{\langle \delta^2 h(0) \rangle} \quad (2)$$

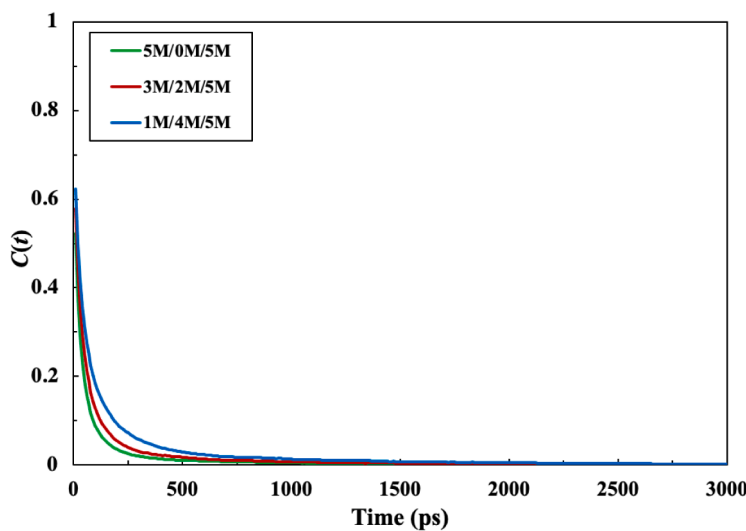
(c) $\text{H}_2\text{O}-\text{O}_{\text{sulfolane}}$

Fig. 8. (continued).

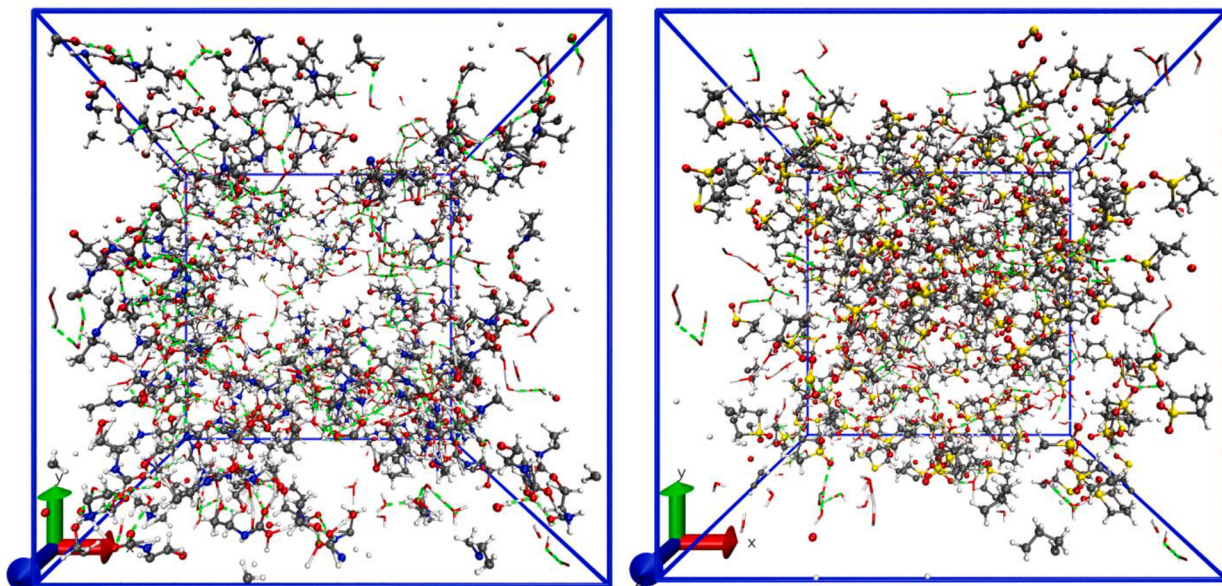


Fig. 9. Distribution of hydrogen bonds between amine products (left) or sulfolane (right) and water in the 3 M/2M/5M. The green lines represent the hydrogen bonds, and the red-white sticks are the water molecules. The details of the structures of amine products can be found in Figure S1 in the Supporting Information.

where, the value of $h(t)$ equals 1 if the atom pair is hydrogen-bonded, and is 0 if not. It should be noted that the $C(t)$ is independent of the breaking of HBs and allows the reformation of the broken HBs[47–49]. As shown in Fig. 8, a large value of $C(t)$ indicates a strong binding nature to water, giving the strength of hydrogen bonds in the order of $\text{MEA}^{\text{COO}}^-$ and water > EAECOO^- and water > sulfolane and water.

The distribution of hydrogen bonds between amine products ($\text{MEA}^{\text{COO}}^-/\text{EAECOO}^-/\text{MEA}^{\text{H}^+}/\text{EAECO}^{\text{H}^+}$) or sulfolane and surrounding water molecules is illustrated in Fig. 9. More hydrogen bonds formed between water and amine products can be found (in Fig. 9 (left)) than that between water and sulfolane (in Fig. 9 (right)), given that the number of amine product molecules and the number of sulfolane molecules are the same ($C_{\text{MEA}} + C_{\text{EAECOO}} = C_{\text{sulfolane}}$). The phenomenon indicates that the formation of hydrogen bonds between water and amine products is more favorable than that between sulfolane and water,

suggesting that the amine products are more strongly solvated by water molecules, which in turns favors the formation of carbamate-waters-protonated amine complex through the hydrogen bond network. Our computational studies based on MD simulations clearly demonstrate that the aggregation of amine products through hydrogen bonding and direct intermolecular interaction, and the self-aggregation of sulfolane on the other side can promote the liquid–liquid phase separation.

4. Conclusions

In this study, a promising monoethanolamine + 2-(ethylamino) ethanol + sulfolane (MEA + EAE + sulfolane) biphasic aqueous solution was developed for the rapid CO_2 absorption and energy-efficient regeneration. The phase separation behavior, CO_2 absorption, and desorption performance, and the position of phase separation point of

the MEA + EAE + sulfolane solutions with different concentration ratios were investigated in experiments. The experimental results indicated that the tunable phase separation property could be achieved by varying the concentration ratios of MEA/EAE/sulfolane. Moreover, the 3 M/2M/5M demonstrated an improved absorption and desorption performance than the benchmark solution (5 M MEA) with a high CO₂ loading of 0.32 mol/mol at the phase separation point. The phase separation mechanism of the MEA + EAE + sulfolane solutions was explored by classical molecular dynamics simulations. The calculation results revealed that the strong hydrogen bonds between amines products and water molecules and the strong intermolecular interaction between amine products would induce the aggregation of amines products/water and self-aggregation of sulfolane, promoting the liquid–liquid phase separation of MEA + EAE + sulfolane solutions after CO₂ absorption. Our combined experimental and computational work may provide key insights into mechanism of liquid–liquid phase separation and the application of amines + organic biphasic aqueous solutions.

Declaration of Competing Interest

The authors declare that they have no known competing financial interests or personal relationships that could have appeared to influence the work reported in this paper.

Acknowledgments

The financial support from the National Natural Science Foundation of China (NSFC-Nos. 22138002, 21978075, 22078083, and 21878073), National Key Research & Development Program - Intergovernmental International Science and Technology Innovation Cooperation Project (2021YFE0112800), Hunan Key R & D Program Project (2020NK2015), the science and technology innovation Program of Hunan Province (2020RC5032), Inner Mongolia Major Science and Technology Major Project (2021ZD0022), the Korea CCS R&D Center (KCRC) grant (No. 2017M1A8A1072016) funded by the Korea government (Ministry of Science, ICT, and Future Planning) and the R. A. Welch Foundation (No. F-1535). We would like to thank the Texas Advanced Computing Center (TACC) at the University of Texas at Austin for providing HPC resources that have contributed to the simulation results reported herein (OCI-1134872).

Appendix A. Supplementary data

Supplementary data to this article can be found online at <https://doi.org/10.1016/j.cej.2022.136674>.

References

- [1] W. Gao, S. Liang, R. Wang, Q. Jiang, Y. Zhang, Q. Zheng, B. Xie, C.Y. Toe, X. Zhu, J. Wang, L. Huang, Y. Gao, Z. Wang, C. Jo, Q. Wang, L. Wang, Y. Liu, B. Louis, J. Scott, A.C. Roger, R. Amal, H. He, S.E. Park, Industrial carbon dioxide capture and utilization: state of the art and future challenges, *Chemical Society Reviews* 49 (23) (2020) 8584–8686, <https://doi.org/10.1039/dcos0025f>.
- [2] Q. Luo, Y. Cao, Z. Liu, B. Feng, Q. Zhou, N. Li, A feasible process for removal and utilization of CO₂ in thermal power plants by MDEA + DMSO scrubbing and Cu/TiO₂ photocatalytic reduction, *Appl. Therm. Eng.* 153 (2019) 369–378, <https://doi.org/10.1016/j.applthermaleng.2019.02.049>.
- [3] G.T. Rochelle, Amine scrubbing for CO₂ capture, *Science* 325 (5948) (2009) 1652–1654, <https://doi.org/10.1126/science.1176731>.
- [4] X. Hu, J. Huang, X. He, Q.L. Luo, C. Li, C. Zhou, R. Zhang, Analyzing the potential benefits of trio-amine systems for enhancing the CO₂ desorption processes, *Fuel* 316 316 (2022) 123216.
- [5] X. Zhang, X. Zhang, H. Liu, W. Li, M. Xiao, H. Gao, Z. Liang, Reduction of energy requirement of CO₂ desorption from a rich CO₂-loaded MEA solution by using solid acid catalysts, *Applied Energy* 202 (2017) 673–684, <https://doi.org/10.1016/j.apenergy.2017.05.135>.
- [6] Q.L. Luo, B. Feng, N. Li, S.C. Liu, A combined experimental and computational study on the shuttle mechanism of piperazine for the enhanced CO₂ absorption in aqueous piperazine Blends, *Industrial & Engineering Chemistry Research* 61 (2022) 1301–1312, <https://doi.org/10.1021/acs.iecr.1c04123>.
- [7] D.J. Heldebrant, P.K. Koech, V.A. Glezakou, R. Rousseau, D. Malhotra, D.C. Cantu, Water-lean solvents for post-combustion CO₂ capture: fundamentals, uncertainties, opportunities, and outlook, *Chemical Reviews* 117 (14) (2017) 9594–9624, <https://doi.org/10.1021/cscs.6b00768>.
- [8] F. Liu, G.T. Rochelle, T. Wang, E. Chen, M. Fang, CO₂ absorption rate in biphasic solvent of aminoethylethanolamine and diethylethanolamine, *Chemical Engineering Journal* 404 (2021) 126503.
- [9] W. Kong, B. Lv, G. Jing, Z. Zhou, How to enhance the regenerability of biphasic absorbents for CO₂ capture: An efficient strategy by organic alcohols activator, *Chemical Engineering Journal* 429 (2022) 132264.
- [10] X. Zhao, X. Li, H. Lu, H. Yue, C. Liu, S. Zhong, K. Ma, S. Tang, B. Liang, Predicting phase-splitting behaviors of an amine-organic solvent–water system for CO₂ absorption: A new model developed by density functional theory and statistical and experimental methods, *Chemical Engineering Journal* 422 (2021) 130389.
- [11] A. Hartono, F. Saleem, M.W. Arshad, M. Usman, H.F. Svendsen, Binary and ternary VLE of the 2-(diethylamino)-ethanol (DEEA)/3-(methylamino)-propylamine (MAPA)/water system, *Chemical Engineering Science* 101 (2013) 401–411, <https://doi.org/10.1016/j.ces.2013.06.052>.
- [12] F. Liu, M. Fang, N. Yi, T. Wang, Research on alkanolamine-based physical-chemical solutions as biphasic solvents for CO₂ capture, *Energy & Fuels* 33 (11) (2019) 11389–11398, <https://doi.org/10.1021/acs.energyfuels.9b02392>.
- [13] S. Zhang, Y. Shen, L. Wang, J. Chen, Y. Lu, Phase change solvents for post-combustion CO₂ capture: Principle, advances, and challenges, *Applied Energy* 239 (2019) 876–897, <https://doi.org/10.1016/j.apenergy.2019.01.242>.
- [14] S. Zhang, Y. Shen, P. Shao, J. Chen, L. Wang, Kinetics, thermodynamics, and mechanism of a novel biphasic solvent for CO₂ capture from flue gas, *Environmental Science & Technology* 52 (6) (2018) 3660–3668, <https://doi.org/10.1021/acs.est.7b05936>.
- [15] F. Liu, M. Fang, W. Dong, T. Wang, Z. Xia, Q. Wang, Z. Luo, Carbon dioxide absorption in aqueous alkanolamine blends for biphasic solvents screening and evaluation, *Applied Energy* 233–234 (2019) 468–477, <https://doi.org/10.1016/j.apenergy.2018.10.007>.
- [16] N. Wang, Z. Peng, H. Gao, T. Sema, J. Shi, Z. Liang, New insight and evaluation of secondary amine/N-butanol biphasic solutions for CO₂ capture: equilibrium solubility, phase separation behavior, absorption rate, desorption rate, energy consumption and ion species, *Chemical Engineering Journal* 431 (2022) 133912.
- [17] W. Zhang, X. Jin, W. Tu, Q. Ma, M. Mao, C. Cui, Development of MEA-based CO₂ phase change absorbent, *Applied Energy* 195 (2017) 316–323, <https://doi.org/10.1016/j.apenergy.2017.03.050>.
- [18] L. Wang, Y. Zhang, R. Wang, Q. Li, S. Zhang, M. Li, J. Liu, B. Chen, Advanced monoethanolamine absorption using sulfolane as a phase splitter for CO₂ capture, *Environmental Science & Technology* 52 (24) (2018) 14556–14563, <https://doi.org/10.1021/acs.est.8b05654>.
- [19] M. Xu, S. Wang, L. Xu, Screening of physical-chemical biphasic solvents for CO₂ absorption, *International Journal of Greenhouse Gas Control* 85 (2019) 199–205, <https://doi.org/10.1016/j.ijggc.2019.03.015>.
- [20] S. Liu, H. Ling, J. Lv, H. Gao, Y. Na, Z. Liang, New insights and assessment of primary alkanolamine/sulfolane biphasic solutions for post-combustion CO₂ capture: absorption, desorption, phase separation, and technological process, *Industrial & Engineering Chemistry Research* 58 (44) (2019) 20461–20471, <https://doi.org/10.1021/acs.iecr.9b03670>.
- [21] J. Lv, S. Liu, H. Ling, H. Gao, W. Olson, Q. Li, Z.A.S. Bairq, Z. Liang, Development of a promising biphasic absorbent for postcombustion CO₂ capture: sulfolane + 2-(methylamino)ethanol + H₂O, *Industrial & Engineering Chemistry Research* 59 (32) (2020) 14496–14506, <https://doi.org/10.1021/acs.iecr.0c02389>.
- [22] R. Wang, L. Jiang, Q. Li, G.e. Gao, S. Zhang, L. Wang, Energy-saving CO₂ capture using sulfolane-regulated biphasic solvent, *Energy* 211 (2020) 118667.
- [23] X. Li, X. Zhou, J. Wei, Y. Fan, L. Liao, H. Wang, Reducing the energy penalty and corrosion of carbon dioxide capture using a novel nonaqueous monoethanolamine-based biphasic solvent, *Separation and Purification Technology* 265 (2021) 118481.
- [24] L. Wang, S. Liu, R. Wang, Q. Li, S. Zhang, Regulating phase separation behavior of a DEEA-TETA biphasic solvent using sulfolane for energy-saving CO₂ capture, *Environmental Science & Technology* 53 (21) (2019) 12873–12881, <https://doi.org/10.1021/acs.est.9b02787>.
- [25] C. Jiang, H. Chen, J. Wang, Y. Shen, J. Ye, S. Zhang, L. Wang, J. Chen, Phase splitting agent regulated biphasic solvent for efficient CO₂ capture with a low heat duty, *Environmental Science & Technology* 54 (12) (2020) 7601–7610, <https://doi.org/10.1021/acs.est.9b07923>.
- [26] X. Zhou, X. Li, J. Wei, Y. Fan, L. Liao, H. Wang, Novel nonaqueous liquid-liquid biphasic solvent for energy-efficient carbon dioxide capture with low corrosivity, *Environmental Science & Technology* 54 (24) (2020) 16138–16146, <https://doi.org/10.1021/acs.est.0c05774>.
- [27] X. Zhou, G. Jing, B. Lv, F. Liu, Z. Zhou, Low-viscosity and efficient regeneration of carbon dioxide capture using a biphasic solvent regulated by 2-amino-2-methyl-1-propanol, *Applied Energy* 235 (2019) 379–390, <https://doi.org/10.1016/j.apenergy.2018.10.118>.
- [28] R. Wang, Y. Yang, M. Wang, J. Lin, S. Zhang, S. An, L. Wang, Energy efficient diethylenetriamine–1-propanol biphasic solvent for CO₂ capture: Experimental and theoretical study, *Applied Energy* 290 (2021) 116768.
- [29] X. Zhang, R. Zhang, H. Liu, H. Gao, Z. Liang, Evaluating CO₂ desorption performance in CO₂-loaded aqueous tri-solvent blend amines with and without solid acid catalysts, *Applied Energy* 218 (2018) 417–429, <https://doi.org/10.1016/j.apenergy.2018.02.087>.
- [30] Q. Luo, B. Feng, Z. Liu, Q. Zhou, Y. Zhang, N. Li, Experimental study on simultaneous absorption and desorption of CO₂, SO₂, and NO_x using aqueous n-

- methyldiethanolamine and dimethyl sulfoxide solutions, *Energy & Fuels* 32 (3) (2018) 3647–3659, <https://doi.org/10.1021/acs.energyfuels.7b03648>.
- [31] A. Dreimanis, Quantitative gasometric determination of calcite and dolomite by using chittick apparatus, *Journal of Sedimentary Research* 32 (1962) 520–529.
- [32] S. Ma'mun, Solubility of carbon dioxide in aqueous solution of potassium sarcosine from 353 to 393K, *Energy Procedia* 51 (2014) 191–196, <https://doi.org/10.1016/j.egypro.2014.07.022>.
- [33] S. Plimpton, Fast parallel algorithms for short-range molecular dynamics, *Journal of Computational Physics* 117 (1) (1995) 1–19, <https://doi.org/10.1006/jcph.1995.1039>.
- [34] G.S. Hwang, H.M. Stowe, E. Paek, D. Manogaran, Reaction mechanisms of aqueous monoethanolamine with carbon dioxide: a combined quantum chemical and molecular dynamics study, *Physical Chemistry Chemical Physics* 17 (2) (2015) 831–839, <https://doi.org/10.1039/c4cp04518a>.
- [35] Q. Luo, R. Dong, B. Yoon, H. Gao, M. Chen, G.S. Hwang, Z. Liang, An experimental/computational study of steric hindrance effects on CO₂ absorption in (non)aqueous amine solutions, *AIChE Journal* (2022), e17701, <https://doi.org/10.1002/aic.17701>.
- [36] K. Dokko, D. Watanabe, Y. Ugata, M.L. Thomas, S. Tsuzuki, W. Shinoda, K. Hashimoto, K. Ueno, Y. Umebayashi, M. Watanabe, Direct evidence for Li ion hopping conduction in highly concentrated sulfolane-based liquid electrolytes, *The Journal of Physical Chemistry B* 122 (47) (2018) 10736–10745, <https://doi.org/10.1021/acs.jpcb.8b09439>.
- [37] G.W.T.M.J. Frisch, H.B. Schlegel, G.E. Scuseria, M.A. Robb, J.R. Cheeseman, G. Scalmani, V. Barone, G.A. Petersson, H. Nakatsuji, X. Li, M. Caricato, A. Marenich, J. Bloino, B.G. Janesko, R. Gomperts, B. Mennucci, H.P. Hratchian, J. V. Ortiz, A.F. Izmaylov, J.L. Sonnenberg, D. Williams-Young, F. Ding, F. Lipparini, F. Egidi, J. Goings, B. Peng, A. Petrone, T. Henderson, D. Ranasinghe, V. Zakrzewski, J. Gao, N. Rega, G. Zheng, W. Liang, M. Hada, M. Ehara, K. Toyota, R. Fukuda, J. Hasegawa, M. Ishida, T. Nakajima, Y. Honda, O. Kitao, H. Nakai, T. Vreven, K. Throssell, J.A. Montgomery Jr., J.E. Peralta, F. Ogliaro, M. Bearpark, J.J. Heyd, E. Brothers, K.N. Kudin, V.N. Staroverov, T. Keith, R. Kobayashi, J. Normand, K. Raghavachari, A. Rendell, J.C. Burant, S.S. Iyengar, J. Tomasi, M. Cossi, J.M. Millam, M. Klene, C. Adamo, R. Cammi, J.W. Ochterski, R.L. Martin, K. Morokuma, O. Farkas, J.B. Foresman, D.J. Fox, Gaussian 09, Gaussian Inc., Wallingford CT, 2016.
- [38] H.M. Stowe, G.S. Hwang, Molecular insights into the enhanced rate of CO₂ absorption to produce bicarbonate in aqueous 2-amino-2-methyl-1-propanol, *Physical Chemistry Chemical Physics* 19 (47) (2017) 32116–32124, <https://doi.org/10.1039/c7cp05580c>.
- [39] H.M. Stowe, E. Paek, G.S. Hwang, First-principles assessment of CO₂ capture mechanisms in aqueous piperazine solution, *Physical Chemistry Chemical Physics* 18 (36) (2016) 25296–25307, <https://doi.org/10.1039/c6cp03584a>.
- [40] A. Einstein, On the movement of small particles suspended in stationary liquids required by the molecular kinetic theory of heat, *Ann. d. Phys* 17 (549–560) (1905) 1.
- [41] W. Humphrey, A. Dalke, K. Schulten, VMD: Visual molecular dynamics, *Journal of Molecular Graphics* 14 (1) (1996) 33–38, [https://doi.org/10.1016/0263-7855\(96\)00018-5](https://doi.org/10.1016/0263-7855(96)00018-5).
- [42] M. Brehm, M. Thomas, S. Gehrke, B. Kirchner, TRAVIS-A free analyzer for trajectories from molecular simulation, *The Journal of chemical physics* 152 (16) (2020), 164105, <https://doi.org/10.1063/5.0005078>.
- [43] M. Brehm, B. Kirchner, TRAVIS - a free analyzer and visualizer for Monte Carlo and molecular dynamics trajectories, *Journal of Chemical Information and Modeling* 51 (8) (2011) 2007–2023, <https://doi.org/10.1021/ci200217w>.
- [44] H. Yoneda, Effect of substitution on dipole moments of molecules, *Bulletin of the Chemical Society of Japan* 31 (6) (1958) 708–714, <https://doi.org/10.1246/bcsj.31.708>.
- [45] W. Zheng, Q. Luo, S. Liu, N. Wang, X. Luo, H. Gao, Z. Liang, New method of kinetic modeling for CO₂ absorption into blended amine systems: A case of MEA/EAE/3DEA1P trisolvent blends, *AIChE Journal* (2022), e17628, <https://doi.org/10.1002/aic.17628>.
- [46] D.C. Rapaport, Hydrogen bonds in water, *Molecular Physics* 50 (5) (1983) 1151–1162, <https://doi.org/10.1080/00268978300102931>.
- [47] T.D.N. Reddy, B.S. Mallik, Hydrogen bond kinetics, ionic dynamics, and voids in the binary mixtures of protic ionic liquids with alkanolamines, *The Journal of Physical Chemistry B* 125 (21) (2021) 5587–5600, <https://doi.org/10.1021/acs.jpcb.0c10658>.
- [48] B. Yoon, G.S. Hwang, On the mechanism of predominant urea formation from thermal degradation of CO₂-loaded aqueous ethylenediamine, *Physical Chemistry Chemical Physics* 22 (30) (2020) 17336–17343, <https://doi.org/10.1039/d0cp02178d>.
- [49] B. Yoon, G.S. Hwang, Anomalous facile carbamate formation at high stripping temperatures from carbon dioxide reaction with 2-amino-2-methyl-1-propanol in aqueous solution, *ACS Sustainable Chemistry & Engineering* 8 (50) (2020) 18671–18677, <https://doi.org/10.1021/acssuschemeng.0c07203>.